Chapter 2

Background

The factors to be considered in the design of bubble column reactors are the fluid dynamics, which involves knowledge of the phase distribution (holdup and bubble size distribution) and velocities (recirculation and turbulence), phase mixing and thereafter the mass and heat transfer characteristics. All these factors put together encompass a broad area of research. Covering all of these in detail is beyond the scope of this work. The goals of this research are the experimental investigation of the fluid dynamics, with specific emphasis on turbulence measurements that can serve in the validation of fundamental fluid dynamic models, and subsequently the use of the experimental information generated in studying and modeling liquid mixing in bubble columns. This information can then be directly used along with bubble size measurements for modeling gas phase mixing and interphase mass transfer, and aid in the design of bubble column reactors.

In view of these goals, the present chapter is divided into four sections. An introduction to the flow phenomena in bubble columns, along with identification of flow regimes and regime transition is covered first. This is followed by a brief description of the approaches used in modeling liquid recirculation in bubble columns. This includes the fundamental hydrodynamic modeling of two-phase flows, using an Euler-Euler approach or an Euler-Lagrange approach, and the phenomenological modeling of liquid recirculation using simplified one dimensional momentum balance equations.

Fundamental modeling of two-phase flows using the Euler-Euler approach requires averaging the microscopic balance equations. This averaging can be performed in different ways (Ishii 1975), resulting in specific forms of the averaged equations. Based on its principle of operation, a given experimental technique provides measurements that correspond to variables in the conservation equations (e.g. velocity and phase holdup) arising from a specific averaging procedure. In the third section of this chapter, the averaging procedures that are commonly used in fundamental modeling and their relation to experimental measurements are discussed. The appropriate averaging procedure of equations required for comparison of model predictions with experimental measurements from CARPT is thereby identified. The advantages and drawbacks of the existing experimental techniques for turbulence measurements in bubble columns are also highlighted in this section. In the fourth section, the existing models in the literature for liquid mixing in bubble columns are reviewed.

2.1 Flow Phenomena

In order to simplify the problem of dealing with the complex flow phenomena in bubble columns, identification of different flow regimes has been introduced (Wallis 1969; Govier and Aziz 1972; Lockett and Kirkpatrick 1975). Flow regimes are known to govern the behavior of the various non-adjustable operating parameters (or system parameters), such as the gas holdup, liquid recirculation, etc. The flow regime depends on column diameter, operating conditions such as superficial gas velocity and pressure, and process variables, such as liquid properties, presence of solids, etc. Three regimes are generally prevalent in bubble column flows as identified by Wallis (1969): i) Bubbly flow regime, or quiescent bubbling, which is characterized by a single size of uniformly distributed bubbles that rise without much interaction; ii) Slug flow regime, which occurs only in small diameter columns (up to 10 cm in diameter), at high gas velocities; iii) Churn-turbulent flow regime, or the heterogeneous flow

regime, which occurs, at higher gas velocities in larger size columns, and is characterized by large and small bubbles, intense turbulence and bubble-bubble interactions (coalescence-redispersion phenomena).

Since slug flow occurs in smaller diameter columns, it is not that commonly encountered in columns of industrial interest. Most attention in the literature has therefore been focussed on the bubbly or homogeneous flow regime and the churn-turbulent or heterogeneous flow regime. The bubbly flow regime has been relatively better understood and characterized (Richardson and Zaki 1954), details of which are found in many reviews on bubble columns, e.g., Shah et al. (1982). Due to the unimodal bubble size distribution, low interaction between the bubbles, and low gas volume fractions (holdups), the bubbly flow regime has been the subject of extensive experimental investigation for studying the instantaneous flow patterns (Chen et al. 1994) and for local measurements involving bubble sizes, phases velocities, etc., using intrusive probes and optical based measurements (Lubbert et al. 1987; Chabot and De Lasa 1993; Groen et al. 1996). For the very same reasons this regime has been the focus of considerable modeling efforts, due to the reduced number of interaction terms in the balance equations in comparison with the churn-turbulent flow regime (Lapin and Lubbert 1994; Sokolichin and Eigenberger 1994; Delnoij et al. 1997).

On the other hand, the churn-turbulent flow regime, with its unstable and chaotic behavior is not quantitatively well characterized. Qualitatively this regime can be described by the presence of large gas bubbles that favor the central portion of the column and rise rapidly (Hills and Darton 1976; Vermeer and Krishna 1981) in the column. This results in a nonuniform radial gas distribution with larger gas holdups at the center than at the wall, which induces liquid recirculation (Devanathan 1991). The smaller bubbles are entrained by the recirculating liquid. In order to understand this flow regime better, and to be able to characterize it quantitatively, experimental information on the bubble sizes, gas holdup distribution, local liquid velocities and turbulence parameters is necessary. Such data are currently scarce owing to the complex and opaque nature this flow regime, which is not conducive to investigations

based on intrusive and optical based techniques (Duduković et al. 1997; Mudde et al. 1997). Non-invasive radiation based techniques for holdup distribution measurements, such as densitometry and tomography, and radioactive particle tracking for liquid/solid velocity measurements have the advantage in this regard, of not being limited by the high gas holdups in the churn-turbulent flow regime. Complex interactions among bubbles, existence of more than one bubble size and intense turbulence have hindered the progress of the fundamental modeling of the fluid dynamics in this regime.

It is, however, the churn-turbulent flow regime that is of industrial interest, due to the necessity for operating at high gas through puts to increase the volumetric productivity (e.g., gas conversion processes). Another factor favoring the churn-turbulent flow regime is the increase in mass-transfer rates when compared to the bubbly flow regime. De Swart (1996) recently showed that the high rates of coalescence and breakup in the churn-turbulent flow regime lead to the rapid renewal of the bubble surface and, thereby, an increase in the gas-liquid interface which increases volumetric mass transfer coefficients. In addition, the high levels of turbulence and liquid recirculation in the churn-turbulent flow regime help in maintaining uniform temperatures in the system, which is favorable for processes involving highly exothermic reactions.

Knowledge of the existing flow regime and identification of the transition between bubbly flow and churn-turbulent flow is necessary to provide a clear picture upon which modeling and design efforts for a particular process can be based. One approach that has been commonly used in identifying the prevailing regime is based on the concept of drift flux, as introduced by Wallis (1969). The drift flux, j_{GL} represents the volumetric flux of gas relative to a surface moving at the volumetric average velocity of the dispersion, $U_g + U_l$, and is given by

$$j_{GL} = U_g\epsilon_l \pm U_l\epsilon_g = u_s\epsilon_g\epsilon_l \tag{2.1}$$

where u_s is the slip velocity between the gas and liquid. A plot of j_{GL} vs ϵ_g reveals the gas velocity at which transition occurs, by an indication of the change in slope of the curve (Figure 2.1). In the bubbly flow regime, which is characterized by a uniform bubble size, the drift flux remains approximately constant with increase in gas velocity and holdup. Upon transition to the turbulent flow regime, the drift increases sharply with gas holdup. Figure 2.1 (a) illustrates with a representative graph the identification of the flow regime. Figure 2.1 (b) shows experimental results for the variation of the drift flux in an air-water system at atmospheric pressure in a 14 cm diameter column. The transition point in Figure 2.1 (b) corresponds to a gas velocity of around 5 cm/s.

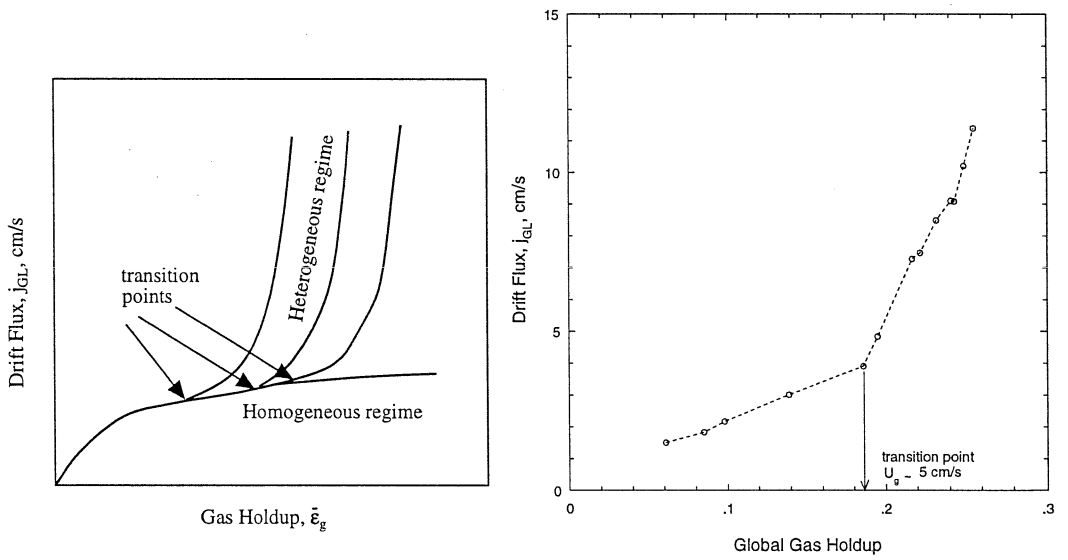

(a) (b)

Figure 2.1: Identification of Flow Regime from Behavior of Drift Flux with Respect to Global Gas Holdup: (a) Schematic Representation (b) Experimental Data from Present Work in a 14 cm Diameter Column

The above method using the drift flux approach enables the evaluation of flow regime transition. The modified drift flux model of Zuber and Findlay (1965) given by

$$\frac{U_g}{\epsilon_g} = C_0(U_g \pm U_l) + C_1 \tag{2.2}$$

is also commonly used to correlate the gas holdup with operating conditions such as the superficial gas and liquid velocities. C_0 and C_1 in Equation 2.2 are constants obtained by fitting the drift flux model to experimental data (reviewed by Joshi et al. 1990).

Based on experimental data from the literature, Deckwer (1980) constructed a flow regime map (shown in Figure 2.2) for air-water systems. For a given system, however, the type distributor can affect the flow regime transition. Due to such effects the boundaries in Figure 2.2 are only approximate. For the experiments conducted as part of the present investigation the transition from bubbly flow to churn-turbulent occurs between 5 to 7 cm/s.

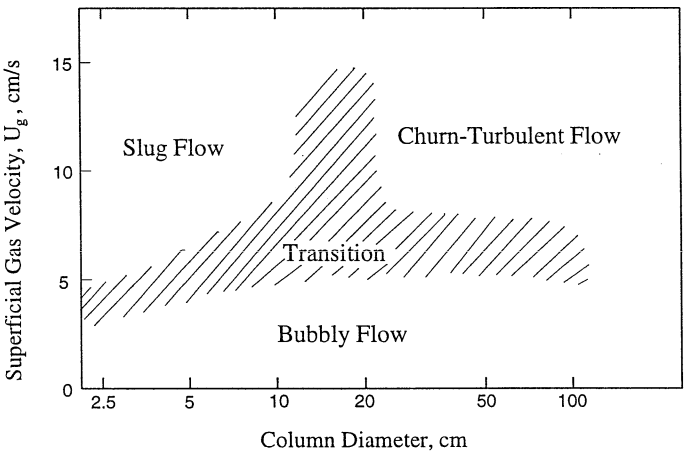

Figure 2.2: Flow Regime Map for Air-Water Bubble Columns (Deckwer 1980)

Transition between flow regimes is strongly influenced by other factors such as change in physical properties of the liquid, presence of solids, increase in system pressure and temperature, etc., which are characteristic of industrial reactors. The influence of these parameters on flow regime transition has been extensively studied by Krishna et al. (1991, 1993) and others (Wilkinson et al. 1992; Reilly et al. 1994) and is a subject of ongoing research (Krishna et al. 1997a). The approach used by these researchers in studying flow regime transition is based on interpretation of gas dynamic disengagement (DGD) experiments.

The DGD technique was originally developed by Sriram and Mann (1977) to study the structure of the gas holdup in bubble columns. They presented a theoretical basis for the technique and showed that the static and dynamic holdups are dictated by the size distributions and rise velocities of the bubbles. A DGD experiment consists of measuring the gas holdup in the column as a function of time, upon shut-off of the gas supply. The holdup measurements are obtained by measuring the dispersion height or by using differential pressure measurements to detect the head in the column (which can be used to calculate the gas holdup). Recently, Shollenberger et al. (1995) have reported the use of nuclear gauge densitometry measurements (a radiation based technique which is discussed in Chapter 6), to measure gas holdup at different axial levels. Analysis of DGD experiments relies on the assumption that there is no bubble-bubble interaction subsequent to gas shut-off. In other words, it assumes that the identity of the bubbles remains unaltered after shut-off of the gas. The change in the gas holdup (or dispersion height) as a function of time, after shut-off of gas supply, is referred to as the disengagement profile. In the bubbly flow regime the disengagement profile generally exhibits a single slope, indicating the existence of a single bubble size distribution. In the churn-turbulent flow regime, with gas velocities greater than 10 cm/s, DGD experiments show two distinct slopes in the disengagement profile. This is interpreted as being caused by the presence of a bi-modal bubble size distribution (Vermeer and Krishna 1981; Schumpe and Grunde 1983; Patel et al. 1989). The initial steep slope of the curve is attributed to the large bubbles that rapidly exit the system, leaving behind the small bubbles that disengage at a much slower rate (second much smaller slope in the disengagement profile). The two slopes of the disengagement curve along with the holdup measurements at the break points in the curve are used to calculate the holdup of the large and small bubbles in the column. Interpretation of DGD experiments with a bi-modal bubble size distribution is based on visual observations and experiments, as mentioned earlier (Hills and Darton 1976). The inherent shortcoming of the model is the assumption of negligible liquid recirculation currents and bubble-bubble interaction immediately after gas shut-off. This may not

be true, especially at very high gas velocities, and such an assumption might influence the quantitative estimates of bubble sizes and rise velocities (Sriram and Mann 1977).

Recently, Deshpande et al. (1995) proposed an alternative single bubble class model to interpret gas disengagement experiments. They argue that the change in slope of the disengagement curve, in the churn-turbulent flow regime, need not arise from the presence of a bi-modal bubble size distribution. Instead, they show that the initial steep drop in the disengagement curve is caused by the decaying of liquid recirculation and the flattening of the gas holdup profile, immediately after gas shut-off. Assuming a one dimensional diffusion model to govern the flattening of the holdup profile, they arrive at time scales for the transition process. They show this time scale to be equivalent to the time taken for the large bubbles (in the model of Vermeer and Krishna (1981) and others) to exit the system. Their model predictions for the disengagement curve are compared against experimental data of Schumpe and Grunde (1986). Based on their model predictions, Deshpande et al. (1995) conclude that the churn-turbulent flow is characterized by a uni-modal bubble size distribution rather than a bi-modal distribution.

Although, the model of Deshpande et al. (1995) has the demonstrated capability to match experimental data, this does not prove the existence of a uni-modal bubble size in churn-turbulent flows, or disprove the existence of a bi-modal bubble distribution. The model in itself is only applied to interpret the initial steep slope of the disengagement curve. However, it does point out the need to account for the liquid recirculation currents that continue to exist even after gas shut-off, even in the bi-modal bubble size model.

Krishna et al. (1991) use the swarm velocity of the bubbles, defined as $\frac{U_g}{\epsilon_g}$, to characterize the transition from the bubbly flow regime to the churn-turbulent flow regime. In the bubbly flow regime, the bubbles are of uniform size and are characterized by a constant swarm velocity. They show that for air (and other gases such as nitrogen and helium) - water systems, the total gas holdup in the bubbly flow regime is characterized by the following linear relationship

$$\text{swarm velocity} \quad = \frac{U_g}{\epsilon_g} = 0.25 \ \text{m/s} \tag{2.3}$$

or

$$\epsilon_g = 4U_g \tag{2.4}$$

In the churn-turbulent flow, due to the presence of both large and small bubbles, $\frac{U_g}{\epsilon_g}$ is no longer constant. The gas velocity at which the swarm velocity, $\frac{U_g}{\epsilon_g}$, starts to increase, denotes the transition velocity. In the churn-turbulent regime the large bubbles constitute the so-called 'dilute' phase (transport holdup), and rise rapidly through the column. The smaller bubbles form the 'dense' phase (entrained holdup) and closely follow the liquid, thereby undergoing recirculation. Such a bi-modal distribution is a characteristic feature of the churn-turbulent flow regime (Krishna et al. 1993). In this regime, the holdup of the small bubbles, or the entrained holdup, remains constant with increase in gas velocity, while the transport holdup of the large bubbles increases. This is schematically represented in Figure 2.3 (Krishna et al. 1991).

Using DGD experiments Krishna and co-workers (1994) have measured the transition gas velocity and contributions of the small bubbles and large bubbles to the overall holdup, and results have been shown to resemble the model represented in Figure 2.3. The effects of pressure were studied by employing gases of varying densities, since an increase in pressure essentially increases the density of the gas phase (Wilkinson 1991; Krishna et al. 1994; Reilly et al. 1994). It was found that an increase in pressure increases the entrained holdup and therefore delays transition. Effects of change in physical properties, such as the density, viscosity and surface tension of the liquid, and the influence of solids on the gas have also been investigated by conducting experiments under various process conditions. Wilkinson et al. (1992) arrived at a correlation to account for the effects of pressure and liquid properties on the transition gas holdup, swarm velocity and transition velocity, (Table 2.1). The basic equation relating the above mentioned parameters is the same as Equation 2.3.

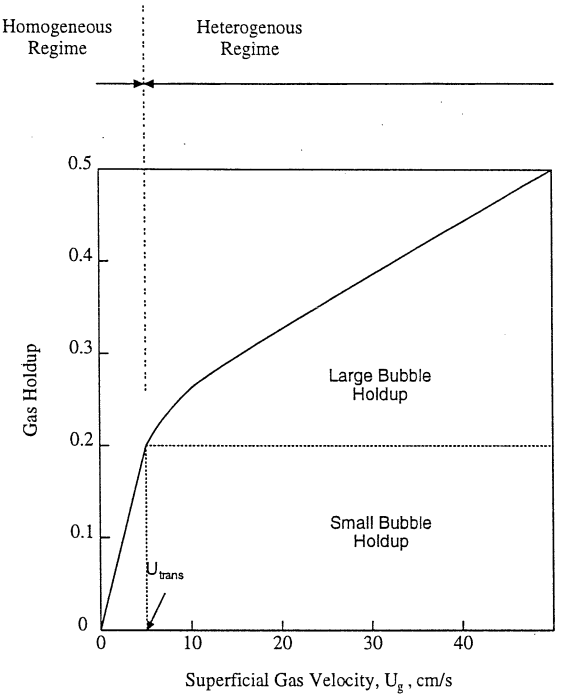

Figure 2.3: Model of Krishna et al. (1991) for Gas Holdup

The correlation of Wilkinson et al. (1992) for the transition velocity and holdup was shown to perform well for systems under high pressures. However, when applied to atmospheric data, Wilkinson's correlation severely underpredicts the transition velocity and holdup to be close to zero. Reilly et al. (1994) have proposed an improved correlation for transition. This correlation fares better than that of Wilkinson et al. (1992) at lower pressures, less than 10 atm. However it overpredicts the transition holdup at very high pressures (discussed in Chapter 6).

Measurements of large bubble holdup and rise velocities, using DGD under different process conditions, have resulted in correlations listed in Table 2.2. The correlation of Krishna et al. (1996) for the large bubbles accounts for column diameter effects, which are believed to be important at very high gas velocities, above 20 cm/s. The correlation of Wilkinson et al. (1992) tends to overpredict the large bubble holdup, especially in large diameter columns (as shown in Chapter 6).

Table 2.1: Correlations for Estimating the Transition Holdup and Transition Gas Velocity based on the Bi-modal Bubble Size Distribution in Churn-Turbulent Flow (SI units)

No.	Reference	
1T.	Wilkinson et al. (1992)	$\epsilon_{trans} = 0.5 \exp\left(-193 \rho_g^{-0.61} \mu_l^{0.5} \sigma^{0.11}\right)$ $\frac{V_{small} \mu_l}{\sigma} = 2.25 \left(\frac{\mu_l^4 g}{\rho_l \sigma^3}\right)^{0.273} \left(\frac{\rho_l}{\rho_g}\right)^{0.03}$ $U_{trans} = \epsilon_{trans} V_{small}$
2T.	Reilly et al. (1994)	$\epsilon_{trans} = 4.457 \sqrt{\frac{\rho_g^{0.96}}{\rho_l} \sigma^{0.12}}$ $V_{small} = \frac{1}{2.84} \frac{1}{\rho_g^{0.04}} \sigma^{0.12}$ $U_{trans} = V_{small} \epsilon_{trans} (1 - \epsilon_{trans})$

Table 2.2: Correlations for Estimating the Large Bubble Holdup and Overall Holdup based on the Bi-modal Bubble Size Distribution in Churn-Turbulent Flow (SI units)

No.	Ref.		
1L.	Wilkinson et al. (1992)	$\frac{V_{lb} \mu_l}{\sigma} = \frac{V_{small} \mu_l}{\sigma} + 2.4 \left(\frac{(U_g - U_{trans}) \mu_l}{\sigma}\right)^{0.757} \left(\frac{\mu_l^4 g}{\rho_l \sigma^3}\right)^{0.077} \left(\frac{\rho_l}{\rho_g}\right)^{0.077}$ $\epsilon_{lb} = \frac{(U_g - U_{trans})}{V_{lb}}$	$\bar{\epsilon}_g = \epsilon_{trans} + \epsilon_{lb}$
2L.	Krishna et al. (1996)	$\epsilon_{lb} = 0.268 \frac{1}{D_c^{0.18}} (U_g - U_{trans})^{0.58}$	$\bar{\epsilon}_g = \epsilon_{lb} + \epsilon_{trans}(1 - \epsilon_{lb})$

A combination of the correlations listed in Table 2.1 and 2.2, for the small bubbles (transition holdup) and large bubbles, are used to calculate the overall gas holdup in the column. Several correlations have been developed earlier, by studying the effects of pressure and liquid properties on the overall gas holdup. Selected ones are listed in Table 2.3. Figure 2.4 shows the gas holdup predictions of the various correlations shown in Tables 2.1 to 2.3, in an air-water bubble column (19 cm in diameter) under atmospheric conditions. There is considerable disparity in the predictions of the various correlations. A possible reason for this is due to the limited database for development of the correlations for each case. For the experimental data considered in this work (Figure 2.4), correlations 3 and 4 in Table 2.3 perform the best. A comparison of the predictions based on the bi-modal bubble size model, shows a vast discrepancy. For atmospheric conditions, a combination of 2T and 2L results in holdup values that are the closest to experimental measurements. However, for high pressure systems, correlation 2T overpredicts the transition holdup. Correlation 1T does better at higher pressures, as shown in Chapter 6.

In addition to the global gas holdup, holdup distribution is also an important variable that is required for determining phase interactions and calculating liquid circulation. While there are extensive measurements of the global holdup under a variety of operating conditions, reports of gas holdup distribution measurements are relatively scarce, due to the requirement for specialized and sophisticated instrumentation. There is knowledge, however, that in bubble columns gas holdup is always larger in the center of the column, than at the walls, and the steepness of the gas holdup profile increases with gas superficial velocity. The existing techniques for measurement of the local void fraction include invasive probes such as the optical fiber probe (De Lasa et al. 1984) and the electrical conductivity probe (Hills 1974; Menzel et al. 1990; Svendsen and Luo 1996), and non-invasive techniques based on absorption and scattering of radiation (x-ray, gamma ray, etc.). A detailed review regarding measurement techniques for local and global measurements is discussed by Kumar et al. (1997).

Table 2.3: List of Correlations for the Global Gas Holdup as a Function of Gas and Liquid Properties (in SI units unless otherwise mentioned)

No.	Reference	Global Gas Holdup, $\bar{\epsilon}_g$
1	Akita and Yoshida (1973)	$\frac{\bar{\epsilon}_g}{(1-\bar{\epsilon}_g)^4} = c(\frac{D_c^2 \rho_l g}{\sigma})^{1/8}(\frac{D_c^3 \rho_l^2 g}{\mu_l^2})^{1/12}(\frac{U_g}{\sqrt{g D_c}})$ c = 0.2 (pure liquids); 0.25 (electrolyte aqueous solutions)
2	Hikita et al. (1980)	$\bar{\epsilon}_g = 0.672(\frac{U_g \mu_l}{\sigma})^{0.578}(\frac{\mu_l^4 g}{\rho_l \sigma^3})^{-0.131}(\frac{\rho_g}{\rho_l})^{0.062}(\frac{\mu_g}{\mu_l})^{0.107}$
3	Hammer et al. (1984)	$\frac{\bar{\epsilon}_g}{1-\bar{\epsilon}_g} = 0.4(\frac{U_g \mu_l}{\sigma})^{0.87}(\frac{\mu_l^4 g}{\rho_l \sigma^3})^{-0.27}(\frac{\rho_g}{\rho_l})^{0.17}$
4	Reilly et al. (1986)	$\bar{\epsilon}_g = 296 U_g^{0.44} \rho_l^{-0.98} \sigma^{-0.16} \rho_g^{0.19} + 0.009$
5	Idogawa et al. (1987)	$\frac{\bar{\epsilon}_g}{1-\bar{\epsilon}_g} = 0.059 U_g^{0.8} \rho_g^{0.17} (\sigma/72)^{-0.22 \exp(-P)}$ P in MPa, σ in mN/m, U_g in cm/s

There exists, at present, no theoretical means of predicting the gas holdup from fundamental equations and all methods rely, to varying extents, on experimental measurements. Fundamental fluid dynamic models, based on the Euler/Euler approach require a holdup distribution at the inlet section of the column to be supplied as input along with information on the bubble size, for modeling of interfacial drag. The only means by which this can be related to the superficial gas velocity is by modeling the distributor (sparger) region, and calculating bubble formation and frequency of formation. Extensive theoretical and experimental work has been done for the case of single bubble formation in stagnant liquids (Azbel 1981; Tsuge 1986; Tan and Harris 1986), which take into account the influence of gas chamber volume on bubble formation. In bubble columns, the formation of gas bubbles at the distributor will, in addition, be affected by the currents in the liquid phase due to the downflowing

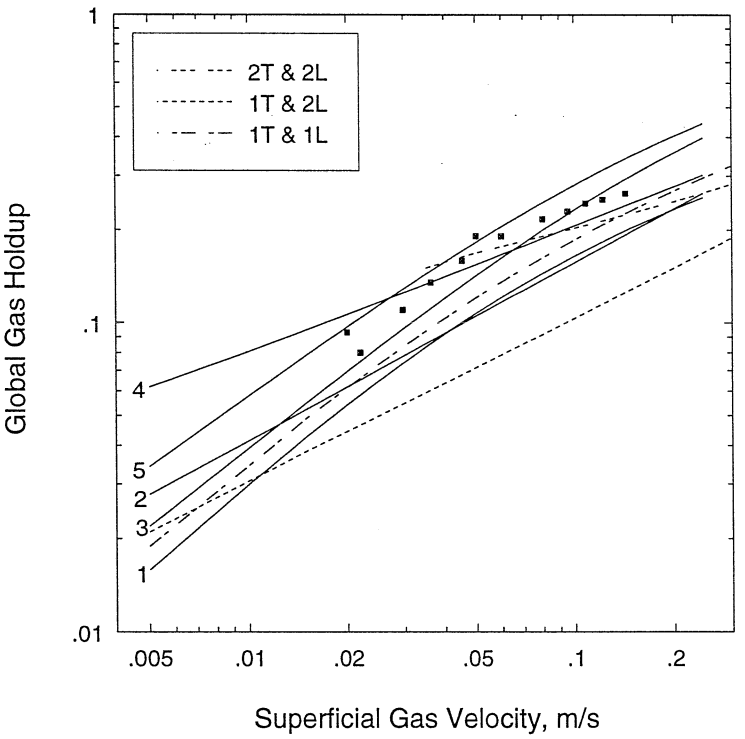

Figure 2.4: Predictions of Literature Correlations for the Global Gas Holdup in a 19 cm Diameter Column, Air-Water System, Atmospheric Conditions (points denote experimental data from present work)

liquid. In such a case, quantitative analyses of bubble formation at the distributor requires coupling of the fluid dynamics in the column with the bubble formation at the distributor.

2.2 Liquid Recirculation

The global gas holdup and above mentioned radial holdup distribution induce liquid recirculation in bubble columns. The gas phase that is introduced at the bottom of the reactor forms bubbles that rise preferentially along the center (axis) of the column, entraining some of the liquid in that region. Liquid rises with the gas phase along the center of the column and descends at the wall, where there are fewer gas

bubbles. Since in bubble column operations the gas superficial velocities are substantially higher than that of the liquid, it is the gas phase that controls the dynamics of the individual phases.

A rigorous approach to modeling the recirculation of liquid is by solving the fundamental Navier-Stokes equations for the individual phases. This approach, known as the Euler-Euler approach (discussed in the following section), requires as an input the gas holdup distribution at the inlet of the column and a typical bubble size for modeling the interfacial drag force between the gas and liquid. In addition, closure models are required for the turbulent stresses and constitutive relations for the gas-liquid interaction terms (drag, lift, virtual mass). Such an approach of modeling is being pursued by several research groups (Svendsen et al. 1992; Jakobsen et al. 1996; Sokolichin and Eigenberger 1994; Ranade 1992; Grienberger and Hofmann 1992; Kumar et al. 1995). Shortage of meaningful experimental data has hindered the successful implementation of these models, especially in churn-turbulent flows.

Another approach in fundamental modeling of gas-liquid flows is the Euler-Lagrange approach. In this formulation the individual bubbles of the gas phase are tracked by writing a force balance for each bubble (Lapin and Lubbert 1994; Delnoij et al. 1997). This is coupled, via the source interaction term and the volume fraction of the gas, with the momentum balance (Eulerian) equation for the liquid phase. This method requires as an input the size of the bubbles, and has so far only been attempted for bubbly flows where there are uniform bubbles without interaction. Euler-Lagrange models do not require turbulence (closure) modeling since they are, at present applied to cases of low gas velocities. For high gas velocities, this approach may not be feasible due to the large number of bubbles that need to be tracked along with multiple bubble interactions.

The solution of fundamental equations, given the complexities involved regarding various closures and computational resources (for three dimensional calculations), remains a subject of current research. Progress in this area requires reliable experimental information for the local fluid dynamic parameters that can serve both for

validation of the models (bubble sizes, phase velocities, holdup distribution and turbulence stresses) and can provide insight into mechanisms that drive the flow.

2.2.1 One Dimensional Recirculation Models

One dimensional recirculation models are based on solving the one dimensional continuity and momentum balance equations, which are simplified versions of the two-fluid model equations (Ishii 1975). These models, as the name suggests, are usually applied to the middle section of bubble columns with aspect ratios larger than 5, where experimental evidence indicates the presence of one dimensional profiles (Devanathan 1991). The model equation, resulting from the conservation of axial momentum, is:

$$-\frac{1}{r}\frac{d}{dr}(r\tau_{rz}) = \frac{dP}{dz} + \rho_l(1-\epsilon_g(r))g \tag{2.5}$$

where

$$-\frac{dP}{dz} = \frac{2\tau_{rz}}{R} + \rho_l(1-\overline{\epsilon_g})g \tag{2.6}$$

ϵ_g is the gas holdup and τ_{rz} is the Reynolds shear stress. Solution of the model equation requires an input for the gas holdup profile, and a closure model for the Reynolds shear stress. Several versions of the one dimensional model have appeared in the literature, which essentially involve the equations shown above (Ueyama and Miyauchi 1979; Clark et al 1987; Anderson and Rice 1989; Rice and Geary 1990; Luo and Svendsen 1991; Kumar et al. 1994). Variations in the models arise from the boundary conditions and closure models used for the Reynolds shear stress, based on Prandtl's mixing length or the eddy viscosity. Although the one dimensional model has been shown to be successful in studying liquid recirculation in bubble columns, the main issue has been in addressing the closure (and scale-up) of the turbulent shear stress, τ_{rz}.

A detailed comparison of the existing approaches using the one dimensional recirculation model to study liquid recirculation in bubble columns, has been performed

by Kumar et al. (1994). Their study demonstrated the deficiency of literature correlations for eddy viscosity and mixing length in satisfactorily predicting the one dimensional liquid velocity profiles under a wide range of operating conditions. They deduced a mixing length scale from the experimental measurements of Reynolds shear stress and liquid velocity gradient, based on which a functional form for the mixing length profile was proposed. It was shown that the mixing length evaluated in a 19 cm diameter column can be used along with the measured holdup profile, to predict recirculation in larger diameter columns, up to 30 cm. Their model was successfully tested for gas velocities ranging from 2 cm/s to 12 cm/s.

The following power law expression was adopted by Kumar et al. (1994) for the gas holdup profile, based on CT (computed tomography) measurements:

$$\epsilon_g(\xi) = \tilde{\epsilon}_g \frac{m+2}{m}(1 - c\xi^m) \tag{2.7}$$

The above expression has been commonly used (with 'c'= 1) to fit the radial holdup profiles (Ueyama and Miyauchi 1979; Rice and Geary 1990). $\tilde{\epsilon}_g$ is related to the cross-sectional average holdup by the following equation:

$$\bar{\epsilon}_g = \tilde{\epsilon}_g \frac{m+2-2c}{m} \tag{2.8}$$

The void fraction exponent 'm', represents the steepness of the holdup profile. This number is usually large ($\geq$ 5) for flat holdup profiles that exist in the bubbly flow regime, and low ($\sim$ 2) in the churn-turbulent flow regime. Parameter c allows for non zero gas holdup at the wall, which is observed from CT measurements (Kumar 1994; Adkins et al. 1996). Such a non-zero value of the gas holdup is also applied in CFD modeling of multiphase flows, using a finite volume scheme, where a non-zero gas holdup is usually calculated in the finite cell volume next to the wall.

The one dimensional model of Kumar et al. (1994) has been used in this investigation for calculating liquid velocity profiles. A detailed explanation of the model and the method of estimating the required parameters is given in Appendix

A. The model is used first to extract information about the mixing lengths, using the time averaged velocity and Reynolds shear stress profiles obtained from CARPT and gas holdup profiles from CT. The model is also used for prediction of liquid recirculation.

2.3 Averaging Procedures in Fundamental Modeling and their Relation to Experimental Measurements

In this section the existing experimental techniques commonly used in two-phase flow measurements are briefly reviewed along with different types of averaging schemes for modeling multiphase flows. The objective is to associate the flow parameters obtained from an experimental technique, based on a brief description of the working principle of the technique, with an averaging scheme used in the fundamental (Euler-Euler) modeling of multiphase flows. The motivation behind performing this exercise is to establish a theoretical basis for the inclusion or omission of certain terms (involving the correlation of the fluctuating holdup), in the averaged conservation equations. The different averaging schemes are discussed first.

2.3.1 Fundamental Modeling: Averaging of Local Instantaneous Equations

Fundamental modeling of multiphase flows, such as gas liquid flows in bubble columns, is commonly based on the two-fluid model (Ishii 1975; Drew 1983), in an Eulerian framework . The two fluid model is formulated based on a continuum mechanics approach, by considering each phase individually. Each phase, therefore, interacts with itself (stress relationship) and with other phases. The conservation laws for each phase are written separately, and the interaction between phases is incorporated via interfacial jump conditions.

Solution of the local instantaneous equations of conservation for each phase along with jump conditions for interfacial interaction is rigorous and complicated due to the moving boundaries of the interface, which requires innumerable initial and boundary conditions. So far, such efforts have been directly applied only for the case of perfectly rigid particles in very dilute suspensions (Sussman et al. 1994). Moreover, for practical applications, analysis in such detail is superfluous. Therefore, the equations are usually averaged before solution. Various types of averaging procedures exist, of which the two most common methods are (1) volume/time averaging (Lahey and Drew 1988) and (2) phasic (time) or ensemble averaging (Ishii 1975; Drew 1983; He and Simonin 1994).

In the first method, averaging is first performed over a control volume, which is larger than the characteristic length scale of the discrete phase, i.e., the bubble size in gas-liquid flows, followed by time averaging of the resulting volume averaged equations. In the second method, the control volume considered is much smaller than the length scale of the discrete phase. Mathematically this can be represented as a point in space.

The various types of averaging procedures and the resulting terms are discussed extensively by Ishii (1975). In what follows, the mathematical implication of the two averaging procedures is considered in terms of the averaged quantities, as they appear in the conservation equations. As an example, the mass conservation equation will be considered. The findings can be extended to terms appearing in the momentum and energy equations.

Volume/Time Averaging

In volume or spatial averaging, the control volume considered is larger than the length scale of the dispersed phase. Consider the local-instantaneous conservation equation for quantity $\rho\psi$ (ψ takes specific values depending on the conservation principle; e.g. $\psi = 1$ for conservation of mass) given by Equation 2.9, that holds at every point in

the flow field, where $\overline{\overline{J}}$ is the flux and $\vec{\phi}$ is the body source per unit mass.

$$\frac{\partial(\rho_k \psi_k)}{\partial t} + \nabla.(\rho_k \psi_k \vec{u}_k) + \nabla.\overline{\overline{J}}_k - \rho_k \vec{\phi}_k = 0 \tag{2.9}$$

The jump conditions applicable at the interface are given by

$$\ll \rho\psi(\vec{u} - \vec{u}_i).\vec{n} - \overline{\overline{J}}.\vec{u} \gg = \overline{\overline{\sigma}}.\vec{n} \tag{2.10}$$

where $\ll \gg$ denotes the jump across the interface moving with a velocity $\vec{u}_i$, and $\overline{\overline{\sigma}}$ represents the surface stresses.

Averaging the equations over the volume occupied by phase k (Figure 2.5), results in instantaneous volume averaged equations (Lahey and Drew, 1988). On volume averaging Equation 2.9 for mass conservation ($\psi = 1$, $\overline{\overline{J}} = 0$, $\vec{\phi} = 0$), one arrives at Equation 2.11 after simplifications (refer to Lahey and Drew (1988) for details). The interfacial jump conditions are transformed into phase interaction terms (Γ_k). Since the control volume is larger than the characteristic length scale of the dispersed phase, spatial averaging results in a phase volume fraction (holdup) at a given instant β_k. Associated with this phase fraction (holdup) is a volume averaged phase velocity $\vec{u}_k$. Equation 2.11 is the instantaneous volume averaged equation for mass conservation.

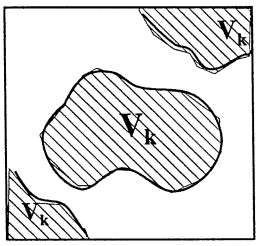

Figure 2.5: Finite Two Dimensional Eulerian Control Volume

$$\frac{\partial}{\partial t}[\beta_k \overline{\rho_k}] + \frac{1}{V}\nabla.[V\beta_k \overline{\rho_k \vec{u}_k}] = \Gamma_k \tag{2.11}$$

where

$$\Gamma_k = -\frac{1}{V}\int_{a_i(\vec{x},t)} \rho_k \vec{n}_k.(\vec{u}_k - \vec{u}_{ki})dS \tag{2.12}$$

V is the Eulerian control volume which is fixed in space and time. Volume averaging is achieved by

$$\overline{f_k} = \frac{1}{V_k(\vec{x},t)}\int_{V_k(\vec{x},t)} f_k(\vec{x'},t)dV' \tag{2.13}$$

and the phase fraction of phase k is

$$\beta_k = \frac{V_k(\vec{x},t)}{V} \tag{2.14}$$

The equation for mass conservation (Equation 2.11), and those for momentum and energy balance (refer to Lahey and Drew (1988)), are volume averaged, yet instantaneous equations. Time averaging is still necessary for solution of these equations for turbulent flows, and is given by

$$\langle \overline{f_k} \rangle = \frac{1}{T}\int_{t-T}^{t} \overline{f_k} dt' \tag{2.15}$$

where $\langle\rangle$ denotes time averaging. For mass conservation, the volume-time averaged mass balance equation takes the final form given below (Lahey and Drew 1988):

$$\frac{\partial}{\partial t}\langle \beta_k \overline{\rho_k} \rangle + \nabla.\langle \beta_k \overline{\rho_k \vec{u}_k} \rangle = \langle \Gamma_k \rangle \tag{2.16}$$

The time averaged velocity of phase k is obtained by:

$$\langle \overline{\vec{u}_k} \rangle = \frac{1}{T}\int_{t-T}^{t} \overline{\vec{u}_k} dt' \tag{2.17}$$

In the above equation, the time interval over which time averaging is performed can be small or large, depending on the type of modeling. Small time scales result in

transient models, while large time scales yield steady state models. The magnitude of the averaging time is not directly apparent, since the final averaged equations do not explicitly contain the averaging time. It is manifested in terms of the frequency or length scales of the turbulent structures. In transient modeling of multiphase flows, the important question is on how to select a (time) window for the time averaging of transient experimental data, in order to quantitatively compare experimental results with model predictions.

The phase density, in Equation 2.16, can be considered to be constant with time and space (incompressible flow), for the case of two phase flows in bubble columns and ρ_k can be brought outside the time averaging operation. Performing Reynolds decomposition of the volume averaged phase velocity and phase holdup we get:

$$\frac{\partial}{\partial t}\rho_k\langle\beta_k\rangle + \nabla.\rho_k[\langle\beta_k\rangle\langle\overline{\vec{u}_k}\rangle + \langle\beta_k'\overline{\vec{u}_k}'\rangle] = \langle\Gamma_k\rangle \tag{2.18}$$

where, for example, $\overline{\vec{u}_k} = \langle\overline{\vec{u}_k}\rangle + \overline{\vec{u}_k}'$, and $\langle\overline{\vec{u}_k}'\rangle = 0$. Similarly $\langle\beta_k'\rangle = 0$. $\overline{\vec{u}_k}$ is obtained from Equation 2.13. Volume-time averaging therefore results in fluctuating holdups β_k', which give rise to the cross-correlation terms involving β_k', such as $\langle\beta_k'\overline{\vec{u}_k}'\rangle$ appearing in the mass conservation equation.

Similarly, starting from Equation 2.9 for the momentum balance ($\psi = \vec{u}$, $\overline{\overline{J}} = pI - T_s$, $\vec{\phi} = g$), volume and time averaging followed by Reynolds decomposition, yields the momentum equation given below. In this equation, the volume and time averaging notation has been dropped for the averaged variables (i.e. for example, $\vec{u}_k$ represents $\langle\overline{\vec{u}_k}\rangle$).

$$\begin{aligned}
&\frac{\partial}{\partial t}\rho_k\beta_k\vec{u}_k + \frac{\partial}{\partial t}\rho_k\langle\beta_k'\vec{u}_k'\rangle + \\
&\nabla.\rho_k\beta_k\vec{u}_k\vec{u}_k + \nabla.\rho_k[\langle\beta_k'\vec{u}_k'\vec{u}_k'\rangle + \beta_k\langle\vec{u}_k'\vec{u}_k'\rangle + \vec{u}_k\langle\beta_k'\vec{u}_k'\rangle + \vec{u}_k\langle\beta_k'\vec{u}_k'\rangle] = \\
&-\beta_k\nabla p - \langle\beta_k'\nabla p'\rangle + \nabla.(\beta_k T_s) + \nabla.\langle\beta_k' T_s'\rangle + F_i + \langle F_i'\rangle
\end{aligned} \tag{2.19}$$

Similar to the mass conservation equation, there are several terms in Equation 2.19 that contain the $\langle \beta_k' \vec{u}_k' \rangle$ term. The $\langle \vec{u}_k' \vec{u}_k' \rangle$ term denotes the Reynolds stress term resulting from volume and time averaging. The above two correlations are collectively referred to as turbulent diffusion terms (Jakobsen 1993). Solution of the above equations will require closure for the various correlations between the fluctuating variables, in addition to constitutive forms for the interfacial coupling term F_i, which includes the drag force, lift and virtual mass forces. T_s represents the viscous shear term.

The volume averaging approach is adopted by several researchers for modeling gas-liquid flows in bubble columns (Torvik and Svendsen 1990; Jakobsen 1993; Grienberger and Hofmann 1992; Ranade 1992; Elgobashi and Abou-Arab 1983; etc.).

Phasic(Time)/Ensemble Averaging

Let us consider the local-instantaneous conservation equation for a conserved quantity $\rho\psi$, as in the previous case, given by Equation 2.9. For the purpose of averaging we consider a small control volume, smaller than the length scale of the discrete phase. In this volume at a given instant in time only one phase can exist. To represent this, consider the phase function $X_k(\vec{x}, t)$, which is defined to be

$$X_k(\vec{x}, t) = \begin{cases} 1 & \text{if } \vec{x} \text{ is in phase } k \text{ at time t} \\ 0 & \text{otherwise} \end{cases} \tag{2.20}$$

X_k is a generalized function and it has been shown to satisfy (Drew, 1983)

$$\frac{\partial X_k}{\partial t} + \vec{u}_i . \nabla X_k = 0 \tag{2.21}$$

∇X_k picks out the interface and causes the discontinuous quantities multiplying it to be evaluated on the phase-k side of the interphase. In order to average Equation 2.9 for each phase k, multiply it by X_k and average it to give

$$\begin{aligned} \frac{\partial}{\partial t}\langle X_k \rho\vec{\psi}\rangle \quad + \quad & \nabla.\langle X_k \rho\vec{\psi}\vec{u}\rangle + \nabla.\langle X_k \overline{\overline{J}}\rangle - \langle X_k \rho\vec{\phi}\rangle = \\ & \langle \rho\vec{\psi}\frac{\partial X_k}{\partial t}\rangle + \langle \rho\vec{\psi}\vec{u}.\nabla X_k\rangle + \langle \overline{\overline{J}}.\nabla X_k\rangle \end{aligned} \tag{2.22}$$

where $\langle f \rangle$ is defined as follows (Ishii 1975):

$$\langle f \rangle(\vec{x}, t) = \frac{1}{T} \int_{t-T}^{t} f(\vec{x}, t')dt' \tag{2.23}$$

or ensemble averaging which can be defined as

$$\langle f \rangle(\vec{x}, t) = \frac{1}{N} \sum_{n=1}^{N} f_n(\vec{x}, t) \tag{2.24}$$

or

$$\langle f \rangle(\vec{x}, t) = \int_{\Omega} f(\vec{x}, t; \omega)d\omega \tag{2.25}$$

where $f(\vec{x}, t; \omega)$ denotes a realization of f over a set of possible equivalent realizations Ω. The three expressions for $\langle f \rangle$ are equivalent when T is very large and alternatively, the number of realizations is large. Equation 2.25 is used by Kashiwa and Gore (1991) in the multi material formalism of the CFDLIB (Computational Fluid Dynamic LIBrary) codes.

If follows that

$$\langle \rho\vec{\psi}\frac{\partial X_k}{\partial t} \rangle = -\langle [\rho\vec{\psi}\vec{u}_i]^k . \nabla X_k \rangle \tag{2.26}$$

Therefore, after simplification

$$\begin{aligned} \frac{\partial}{\partial t}\langle X_k \rho\vec{\psi} \rangle + \nabla . \langle X_k \rho\vec{\psi}\vec{u} \rangle + \\ \nabla . \langle X_k \overline{\overline{J}} \rangle - \langle X_k \rho\vec{\phi} \rangle \quad = \quad \langle [\rho\vec{\psi}(\vec{u} - \vec{u}_i) + \overline{\overline{J}}]^k . \nabla X_k \rangle \end{aligned} \tag{2.27}$$

The above equation can be reduced to represent mass, momentum and energy balance. For mass balance, taking $\vec{\psi}_k$=1, $\overline{\overline{J}} = \vec{\phi} = 0$, Equation 2.27 reduces to

$$\frac{\partial}{\partial t}(\alpha_k \langle \rho_k \rangle^x) + \nabla . \alpha_k \langle \rho_k \rangle^x \langle \vec{u}_k \rangle^{x\rho} = \underbrace{\langle [\rho(\vec{u} - \vec{u}_i)]^k . \nabla X_k \rangle}_{interfacial\ mass\ exchange\ term} \tag{2.28}$$

where holdup of phase k (the fraction of time spent at a given point by phase k, or the local volume fraction of phase k) is given by

$$\alpha_k = \langle X_k \rangle \tag{2.29}$$

$$\langle \rho_k \rangle^x = \langle X_k \rho \rangle / \alpha_k \tag{2.30}$$

$$\langle \vec{u}_k \rangle^{x\rho} = \langle X_k \rho u \rangle / \alpha_k \langle \rho_k \rangle^x \tag{2.31}$$

Equation 2.30 is the definition of phasic averaging, and Equation 2.31 is for mass-weighted averaging, also known as Favre averaging (1965). In multiphase flows of interest, such as in bubble columns, usually the density of each phase is constant (incompressible flows), therefore the mass-weighted average reduces to phasic averaging, and we have

$$\frac{\partial}{\partial t}(\rho_k \alpha_k) + \nabla . \alpha_k \rho_k \langle \vec{u}_k \rangle^x = \underbrace{\langle [\rho_k (\vec{u} - \vec{u}_i)]^k . \nabla X_k \rangle}_{interfacial\ mass\ exchange\ term} \tag{2.32}$$

The instantaneous phase velocity can be decomposed into its phasic averaged velocity and a corresponding fluctuation,

$$\vec{u}_k = \langle \vec{u}_k \rangle^x + \vec{u}_k'' \tag{2.33}$$

$$\langle \vec{u}_k'' \rangle \neq 0 \tag{2.34}$$

$$\langle \vec{u}'' X_k \rangle = 0 \tag{2.35}$$

Hence, due to the basic definition of α_k, cross-correlation terms of the fluctuating holdup with fluctuating velocity do not arise in the phase averaged mass conservation equation (Equation 2.32), or other averaged conservation equations. Such a type of phasic or ensemble averaging is adopted in the formulation of the CFDLIB codes (Kashiwa and Gore 1991), and by others (Sokolichin and Eigenberger 1994).

In order to compare the averaged velocities resulting from the above two averaging procedures it is first necessary to volume average the above phase averaged velocities.

$$\overline{\langle \vec{u}_k \rangle^x} = \frac{\overline{\langle X_k \vec{u} \rangle}}{\overline{\alpha}_k} \tag{2.36}$$

but

$$\overline{\langle X_k \vec{u} \rangle} = \frac{1}{V} \int_V \{ \frac{1}{T} \int_{t-T}^{t} X_k u dt' \} dV = \frac{1}{T} \int_{t-T}^{t} \{ \frac{1}{V} \int_{V_k} \vec{u}_k dV \} dt' = \langle \beta_k \overline{\vec{u}_k} \rangle \tag{2.37}$$

and

$$\langle \beta_k \rangle = \overline{\alpha_k} \tag{2.38}$$

Therefore, after simplification we get

$$\overline{\langle \vec{u}_k \rangle^x} = \langle \overline{\vec{u}_k} \rangle + \frac{\langle \beta_k' \overline{\vec{u}_k}' \rangle}{\langle \beta_k \rangle} \tag{2.39}$$

Equation 2.39 gives the relationship between the volume-time averaged phase velocity and the phasic averaged-volume averaged velocity. These two velocities are different from each other, and hence affect the final form of the conservation equations.

An equivalent analysis for the momentum balance equation yields the following relationship between the Reynolds stresses arising from the volume averaged equation and the phasic averaged equation:

$$\langle \vec{u}_k'' \vec{u}_k'' \rangle^x = \langle \vec{u}_k' \vec{u}_k' \rangle + \frac{\langle \beta_k' \vec{u}_k' \vec{u}_k' \rangle}{\langle \beta_k \rangle} - \frac{\langle \beta_k' \vec{u}_k' \rangle \langle \beta_k' \vec{u}_k' \rangle}{\beta_k^2} \tag{2.40}$$

where $\langle \vec{u}_k'' \vec{u}_k'' \rangle^x$ is the phasic averaged turbulent Reynolds stress and $\langle \vec{u}_k' \vec{u}_k' \rangle$ is the Reynolds stress based on volume and time averaging.

In the following section the averaged fluid dynamic quantities such as the phase holdup and velocity, as measured by different techniques, are related to the corresponding quantities resulting from the different averaging procedures discussed

above. A brief description of the operating principle of each experimental technique is given, along with merits and drawbacks of the technique and applications to bubble column measurements, reported in the literature.

2.3.2 Measurement Techniques for Fluid Dynamic Parameters

The existing experimental techniques that have been considered for measurement of the various multiphase fluid dynamic parameters are as follows. For liquid velocity:

- Pitot Tube
- Flywheel Anemometry
- Heat Pulse Anemometry
- Hot Film (Wire) Anemometry
- Laser Doppler Anemometry (Velocimetry)
- Particle Image Velocimetry
- Computer Automated Radioactive Particle Tracking (CARPT)

For gas holdup, bubble size and rise velocity:

- Optical Fiber Probe
- Ultrasound Doppler
- Computed Tomography
- Electrical Impedance probes like conductivity, capacitance, etc.

Velocity measurements

Pitot Tube

The Pitot tube is a classical device used for measuring the velocity in single phase flows. The principle of the Pitot tube is based on measuring the difference between the static pressure and dynamic pressure at a given point in the flow field. For measurement in two phase flows the above equation has to be modified. Details for adaptation of this device to two phase flow are discussed elsewhere (Hills 1974; Euzen et al. 1993). Essentially in all cases the holdup should be known at the instant of measurement of the differential pressure, from which the liquid velocity is deduced using simplified assumptions for the phase coupling. Usually pseudo-homogeneous flow of gas and liquid is assumed. This assumption becomes questionable in churn-turbulent flows. The accuracy of these measurements is also limited by the difficulty in measuring two phase differential pressure. Hills (1974) used a modified Pitot tube to measure the liquid phase velocities in a bubble column of diameter 14 cm up to gas velocities of 17 cm/s. His measurements were amongst the first for local averaged liquid velocities and holdups in bubble columns. Pitot tube measurements, which are based on measuring the differential pressure at a given location using the local holdup for interpretation, yield a volume averaged liquid velocity (Equations 2.13 and 2.15).

Flywheel Anemometry

The fly wheel anemometer falls under the class of turbine flow meters. As the name suggests it is based on measuring the rotational speed of a flywheel induced by the flowing liquid. The implicit assumption is that due to the large difference between liquid and gas densities, the momentum of the flowing liquid on the flywheel far exceeds that of the flowing gas. This may become questionable at high gas superficial velocities in bubble columns due to the large gas holdups present, or at high pressures which increases the gas density. Despite this limitation, the flywheel anemometer was successfully applied by Nottenkamper et al. (1983) to measure the local average liquid

phase velocities, in large diameter (45 and 100 cm) bubble columns up to very high gas velocities (80 cm/s), well in the churn-turbulent flow regime.

This type of measurement, which measures continuously in time the velocity of the volume of liquid flowing through the flywheel, results in volume/time averaged liquid phase velocities, given by Equation 2.15.

Heat Pulse Anemometry

The Heat Pulse Anemometry (HPA) technique was developed by Lubbert and Larson (1990) to measure the time averaged liquid velocity, based on time-of-flow measurements. The method relies on using heat as a tracer. Fluid elements are tagged by direct local ohmic heating using a high frequency alternating current between two small electrodes placed in the reactor. The dispersion of heat is measured a small distance away from the source of heat using a hot-film anemometer which acts as a temperature detector. The signal to noise ratio of the device is increased by using as input a pseudo-random sequence of heat pulses, rather than a single impulse input. Information regarding the time-of-flow distribution is obtained from the cross-correlation between the input and output signals. The liquid velocity between the probes can be estimated from the mean time-of-flow and the distance between the emitter and sensor probes. The technique rests on the assumption that in the time averaged sense the probes are placed along the liquid velocity streamlines (Lubbert and Larson 1990).

Hot Film Anemometry (HFA)

Hot wire or film anemometry (HWA/HFA), is a technique which utilizes the resistance change in an electrical resistance wire, or film supported on a base, due to the removal of heat by a flowing fluid. The heat flux from the heated cylinder to the ambient fluid is determined by the velocity, the physical properties of the fluid and the temperature difference between the fluid and the sensor probe. In addition to being widely used for the measurement of liquid velocities in single phase flows, HFA has also been

applied for measurement of liquid velocities in two phase gas-liquid flows (Delhaye 1969; Serizawa et al. 1975; Herringe and Davis 1974). Franz et al. (1984) and Yao et al. (1991) used the HFA to measure the averaged velocities and turbulent normal stresses in bubble columns. Menzel et al. (1990) developed a triple split fiber HFA (multiple point probes are necessary to simultaneously measure the different components of the liquid velocity) to measure the Reynolds shear stress, in addition to the average velocities in bubble columns. Using this technique requires calibration of the setup in a preconditioned flow in order to assess the exact relationship between the heat loss and the relevant variables.

The size of the probe is typically very small. For example, the size of the probe used by Menzel et al. (1990) for bubble column flows was about 2 mm long and 500 μm in diameter. At a given instant in time, the probe senses either the presence of liquid or gas. In order to measure the velocity of a particular phase, it is first necessary to distinguish between the phases, from the signal obtained. This issue has been addressed by several researchers (for example, Delhaye (1969), Serizawa et al. (1975), Herringe and Davis (1974)), who have developed criteria for distinguishing the signal when the probe is in the liquid phase, by which, active measurements of the velocity are recorded only when the probe senses the liquid. The local average liquid velocity is hence "weighted" by the number of times the probe tip senses the liquid phase. The average velocities and corresponding turbulent intensities are therefore based on phasic averaging (Equations 2.31, with constant density, and 2.33).

Difficulties in using the HWA arise, especially at higher gas velocities in churn-turbulent flows, due to incomplete piercing or sliding of bubbles on the probe, when signal processing becomes more complex. Despite these complexities, HWA and HFA have been widely used to measure the liquid phase velocities and turbulence in bubble columns. Franz et al. (1984) used the HFA for measuring the average and fluctuating rms liquid velocities in a 14 cm diameter column with continuous flow of liquid ($U_l =$ 2 cm/s). By varying the orientation of the probe they were able to measure the three components of the velocity, and showed that the assumption of axisymmetric flows in

bubble columns is not valid. Their measurements indicated the presence of "structural elements or vortices" even in the time averaged sense. Menzel et al. (1990) developed a triple split probe, by which they were able to simultaneously measure the radial and axial components of the instantaneous liquid velocity. This enabled the measurement of Reynolds shear stress in a 15 cm and 60 cm diameter column. They report errors to a maximum of 30 % for the turbulence measurements. Their measurements were amongst the first (along with CARPT measurements of Devanathan (1991)) for the Reynolds shear stresses. The turbulent shear stress measurements of Menzel et al. (1990) in the 15 cm column are used as a reference in the present investigation, against which CARPT measurements are validated.

Laser Doppler Anemometry (LDA)

Laser Doppler Anemometry (LDA) is a well established technique for velocity measurement in single phase flow (Durst et al. 1981), and has the advantage over HFA in that no tedious calibration is required. The experimental setup consists of using two monochromatic, coherent polarized beams of light which intersect at a specific angle within the flow domain of interest, to form a small measuring volume. In this region the wave fronts overlap and interference fringes form throughout the entire measurement volume which is typically very small. The liquid is seeded with minute tracer particles (0.5 to 5 μm) which follow the motion of the fluid. When a particle flows through the measuring volume, the light is scattered in a characteristic manner. The frequency of this scattered light is referred to as the Doppler frequency. The particle velocity U is related to this Doppler frequency f_D, the intersection angle between the incident laser beams and the wavelength λ of the beams given by:

$$U = \frac{f_d \lambda}{2 \sin(\theta/2)} \tag{2.41}$$

As is obvious from Equation 2.41, for a given wavelength and angle of intersection, the Doppler frequency is directly related to the particle velocity, and therefore

no calibration is required. For simultaneous measurement of two components of the velocity in the measurement of shear stresses, a beam separator or splitter is used which generates a two dimensional reference beam from which two components of the velocity can be measured (Durst et al. 1981; Groen et al. 1996).

As with the case of HFA, in two phase gas-liquid flows suitable procedures are applied to distinguish between the two phases in the raw signal from LDA. This ensures that only the liquid phase velocities are measured in the measuring volume which is typically smaller than the size of the bubbles (Lance and Bataille 1991, Groen et al., 1995). The resulting signal is therefore similar to the local measurement of the liquid velocity using HFA, thereby yielding phasic averages of the liquid velocities (Equation 2.31) and corresponding correlations of the fluctuating velocities.

The major drawback of LDA in two-phase flow is the scattering caused by the bubbles in the flow, which should not be misinterpreted as signals from the liquid phase. For this reason, the LDA is restricted to conditions of low gas holdup in small diameter columns at low gas velocities (bubbly flow regime), or near the wall region in larger size columns and higher gas velocities.

LDA and HFA can theoretically be used to measure the local time average holdups. However, multiple scattering of the signal in LDA, and similar signal processing errors in HFA, can lead to erroneous values for the gas holdup, which makes these results unreliable. Therefore LDA (and HFA) is typically applied only measure the liquid velocities (Mudde et al. 1997).

Mudde and coworkers (Groen et al. 1996; Mudde et al. 1997) have developed and used the LDA for measurement of the axial and tangential components of the liquid velocity in 15 cm and 23 cm diameter bubble columns. In the larger column they obtained measurements only close to the wall ($\geq$ 0.7 R). The LDA has the advantage of being able to capture frequencies up to 500 Hz. By calculating the auto power spectral density of the time series, they showed that the spectra obey the -5/3 power law of Kolmogorov, suggesting that at small wave numbers the cascade of turbulence is not significantly affected by the presence of bubbles. The experimental

results for turbulence measurements from the present investigation, using CARPT, have been successfully compared with LDA results of Mudde et al. (1997) (discussed in Chapter 4).

Particle Image Velocimetry (PIV)

Particle Image Velocimetry (PIV) falls in a broad class of particle-imaging techniques used for flow visualization (Adrian 1991) in which the motion of small marked regions of a fluid is measured by observing the locations of the images of the markers at two or more times. In the PIV technique, a laser sheet is used to illuminate a two dimensional plane of the flow field. Small neutrally buoyant (seeding) particles used to trace the liquid are illuminated by the sheet of light. The particles scatter light, which is recorded by a camera at 90^o to the sheet of light. The gas bubbles in the flow are self-illuminated by the laser sheet. Data processing of subsequent frames results in the calculation of instantaneous Lagrangian phase velocities in the 2-D illumination plane.

Fan and coworkers (Tzeng et al. 1993; Chen et al. 1994) have used PIV in two dimensional and three dimensional bubble columns and fluidized beds to measure instantaneous phase velocities as well as phase holdups. From the instantaneous velocities, the averaged flow field can be calculated by recording the images of the flow field over a large number of times, and ensemble averaging the resulting flow parameters such as velocities, turbulence intensities, and phase holdups at a given location (volume). Such averaging is similar to the procedure employed in the CARPT technique and results in phasic averaged velocities, as shown in the following section. The limitation of the PIV technique, similar to LDA, is that it is can be successfully used only in modest column diameters and at low gas velocities, since it is an optically based technique.

Computer Automated Radioactive Particle Tracking (CARPT)

In the CARPT technique (Devanathan et al. 1990) the position of a neutrally buoyant particle, which tracks the liquid phase, is measured over a certain period of time. Time differencing of the successive particle positions gives the Lagrangian velocity. These Lagrangian velocities are used to calculate the time averaged velocities of the liquid at different positions in the column. For the purpose of the present objective, which is to determine the nature of the averaged quantities resulting from CARPT measurements, a brief description of the data processing involved is provided. A detailed version is presented in Chapter 3, which discusses various aspects of the CARPT technique. The column is divided into compartments. The velocity of the particle is then assigned to that compartment which contains the mid-point of the two successive positions of the particle. In this manner instantaneous velocities are assigned to their respective compartments. Ensemble averaging is done by averaging the velocities in a given compartment over the number of times (repetitions) that the particle visits that compartment. If N_{vel} is the number of repetitions in a given compartment, the ensemble average liquid velocity component along the i^{th} direction in that compartment is

$$\langle u_i \rangle = \frac{1}{N_{vel}} \sum_{j=1}^{j=N_{vel}} u_{i,j} \tag{2.42}$$

where $u_{i,j}$ is the j^{th} assignment of the i^{th} velocity component to that compartment resulting from the j^{th} visit of the particle. Invoking the ergodic hypothesis, ensemble averaging yields time averaging. Therefore $\langle u_i \rangle$ is the time averaged liquid velocity in the given compartment. Typically, the volume of the compartment is larger than the length scale of the discrete phase, similar to the volume V used in the volume/time averaging method (refer to Equation 2.15 and Figure 2.5).

Rewriting Equation 2.15 in discretized form for component i of the liquid phase velocity, gives

$$\langle\overline{u_i}\rangle = \frac{1}{N_T}\sum_{j=1}^{j=N_T}\frac{1}{N_{V_l}(j)}\sum_{l=1}^{l=N_{V_l}(j)} u_{i,j,l} \tag{2.43}$$

N_T is the number of time steps over which time averaging is performed. i denotes the ith component of the velocity vector and $u_{i,j,l}$, the local (l), instantaneous (j) velocity of the liquid phase. N_{V_l} represents the number of discrete points that comprise the volume V_l occupied by the liquid phase, which in transient flows such as in bubble columns changes with time, i.e., N_{V_l} = f(time or 'j'). Therefore volume/time averaging given by Equations 2.15 and 2.43 is not compatible with the results from CARPT.

The other averaging method is phasic averaging. Volume averaging of the phasic averaged velocity given by Equation 2.36, again for component i of the liquid phase velocity, when rewritten in discretized form, gives

$$\overline{\langle u_i\rangle^x} = \frac{\frac{1}{N_V}\sum_{j=1}^{j=N_V}\frac{1}{N_T}\sum_{l=1}^{l=N_T} X_l u_i}{\frac{1}{N_V}\sum_{j=1}^{j=N_V}\frac{1}{N_T}\sum_{l=1}^{l=N_T} X_l} = \frac{\sum_{j=1}^{j=N_V}\sum_{l=1}^{l=N_T} X_l u_i}{\sum_{j=1}^{j=N_V}\sum_{l=1}^{l=N_T} X_l} \tag{2.44}$$

where X_l is the phase function for the liquid phase (Equation 2.20), N_T is the number of samples acquired over a given time interval (t-T to t) and N_V is the number of discrete points that comprise the averaging (control) volume V. Both N_T and N_V are fixed values and therefore constant.

Equation 2.44 implies that for a given control volume V, $\overline{\langle u\rangle^x}$ is the arithmetic average of all the velocities measured for the liquid phase over N_T time steps and N_V volume samples. This represents the discretized version of Equation 2.36, and is the same as the (ensemble) time averaged velocity obtained from Equation 2.42, where

$$N_{vel} \rightarrow \sum_{j=1}^{j=N_V}\sum_{l=1}^{l=N_T} X_l \text{ as } N_{vel} \rightarrow \infty \ \ (\infty \cong 500) \tag{2.45}$$

Since $X_l = 0$ in the presence of the gas phase at a given location, the double summation in Equation 2.44 can be approximated by a single summation over N_{vel}. Therefore, the CARPT measurements which result in time averaged liquid velocities in a

compartment volume are equivalent to the phasic averaged velocities averaged over the control volume V as given by Equation 2.36. PIV measurements (same principle of averaging as CARPT) result in similar averaged velocities.

Techniques such as HFA and LDA. as discussed before, result in local phasic averages of the liquid phase velocities. Therefore the four, noted experimental techniques for instantaneous liquid velocity measurements, i.e., HFA, LDA, CARPT and PIV yield the same type of averages. While HFA and LDA are local, CARPT and PIV yield a volume average of the phasic averaged velocities.

Gas holdup, bubble size and rise velocity measurements

The basic definition of the average gas holdup suggests that both types of averaging yield the same average holdup (Equation 2.38). Therefore, all experimental measurements should yield the same result for the average holdup.

Intrusive probes, such as the optical fiber probe (Nottenkamper et al. 1983; De Lasa et al. 1984; Groen et al. 1996) and electrical impedance probes (electrical conductivity probe: Hills (1974), Menzel et al. (1990), Yao et al. (1991), Svendsen and Luo (1996)), and the non-intrusive Ultrasound Doppler (Lubbert et al. 1987) measure the time averaged local gas holdup, defined as the fraction of time that the probe senses the gas phase (α_g). These probes are also used to measure bubble sizes based on the pierced chord length. However, such measurements are prone to error at higher gas velocities due to the non-spherical shapes of the bubbles and the randomness in their trajectories. Groen et al. (1995) show that the orientation of the optical fiber probe results in different results for the local average holdup measurements. Extensions of the single point optical fiber and conductivity probes (using multiple split fiber probes) have been used to measure the bubble rise velocities with some success (Yao et al. 1991; Svendsen and Luo 1996; Chabot 1993; Groen et al. 1995).

Volume averaged phase holdups usually result from non-invasive techniques, such as densitometry and tomography. Computed Tomography (CT) measurements

using γ radiation (Kumar, 1994) result in time and volume averaged holdups ($\overline{\beta_g}$). In principle instantaneous measurements of the volume averaged holdup, β_g, are possible. However, in practice, owing to the noise in the data arising from the statistical fluctuations of the radiation only time averaged holdups are feasible. By using high energy and high strength sources, it may be possible to obtain instantaneous measurements of β. Electrical impedance tomography, based on measuring the electrical resistance in the flow between pairs of electrodes which are spaced around the test section, seems to show promise in measuring the instantaneous volume fractions (Dickin et al. 1993). The spatial resolution of this technique is, however, limited by the uncertainties in the flow pattern and lack of uniformity of electrical properties. Nevertheless, it would be possible to obtain β_g' using such a measurement technique (O'Hern et al. 1995).

In order to use the results from experimental measurements for liquid velocities, turbulence parameters and phase holdups from the above mentioned techniques, for comparison with model predictions, based on the above analysis, it seems appropriate to use the phasic or ensemble averaging scheme for averaging the two-fluid model equations, since most experimental measurements correspond to this type of averaging. Phasic averaged equations in their exact form do not give rise to a fluctuating gas holdup term and corresponding correlations in the balance equations. If, for gas-liquid flows in bubble columns, $\langle \beta_g' u_g' \rangle$ is negligible (~ 0), then the two types of averaging will result in the same final averaged equations.

In Chapter 6, phasic averaging of the liquid tracer species balance equation is used to develop a two dimensional model for liquid mixing in bubble columns. The phase fractions, α_k and β_k have been used only in this section for the sake of analysis. In the remaining chapters, ϵ_k is used to denote holdup of phase k.

2.4 Liquid Mixing

The complex flow phenomena in bubble columns complicates phase mixing and other transport processes. Liquid mixing on the macroscale is a resultant of various contributing mechanisms. These are:

- Global convective recirculation of the liquid phase which is induced by the non-uniform gas radial holdup distribution
- Turbulent diffusion due to the eddies generated by the rising bubbles. This factor is an overall contribution due to turbulence which comprises of:
  - Large scale fluctuations caused by the large scale eddies.
  - Small scale fluctuations arising from the entrainment of liquid in the wakes of the fast rising bubbles
- Molecular diffusion, which in comparison to the above factors is negligible.

2.4.1 The Axial Dispersion Model

The most common approach to modeling the non-ideal mixing behavior in bubble columns is the one dimensional axial dispersion model. In this model, all the above mentioned mechanisms leading to liquid macromixing are lumped into a single axial dispersion coefficient. The immense popularity of the model is due to its simplicity and ease of use. However, the validity of the axial dispersion model to describe two-phase flows with large degrees of backmixing, such as those in bubble columns is somewhat questionable (Wen and Fan 1975; Rice et al. 1981). Several researchers (Levenspiel and Fitzgerald 1983; Hatton and Lightfoot 1984) have cautioned against the use of the ADM for bubble column flows. Hatton and Lightfoot (1984) approached the problem of dispersion and mass transfer from a generalized dispersion framework and, through a complex analysis showed that a simple one dimensional axial dispersion model is incapable of describing dispersion in multiphase systems. Myers (1986)

has presented a detailed analysis of the objections to the axial dispersion model for bubble columns, where he shows that there is no basis for the use of the ADM in bubble columns. Despite the lack of a sound basis for application to bubble columns, the ADM still remains extremely popular and numerous correlations for the liquid axial dispersion coefficient in bubble columns have been developed over the years. Available literature correlations are listed in Table 2.4. Table 2.5 lists the sources of experimental data based on which most of the correlations were developed. Essentially, all the experimental data for the axial dispersion coefficient are for air-water at atmospheric conditions (Shah et al. 1978). The range of gas velocities covers both the bubbly flow and churn-turbulent flow regime. The number of experimental data points obtained in the churn-turbulent regime is rather limited in comparison with bubbly flow.

Most correlations express the axial dispersion coefficient as a function of superficial gas velocity and column diameter, while in some cases the physical properties of the liquid have also been accounted for. The majority of these correlations are entirely empirical. There have been, however, attempts made to derive a theoretical or semi-theoretical relation for the axial dispersion coefficient based on various approaches. A brief discussion of the concepts involved in the various analyses presented in the literature is given here. An extensive review on this subject has been presented by Kastanek et al. (1993).

Baird and Rice (1975) assumed the validity of Kolmogorov's theory of isotropic turbulence and by dimensional analysis showed that the axial dispersion coefficient can be expressed by:

$$D_{ax} = K_r l_e^{\frac{4}{3}} P_m^{\frac{1}{3}} \tag{2.46}$$

where l_e is the characteristic length scale of the eddies that are primarily responsible for eddy diffusion. P_m, the specific energy dissipation rate per unit mass, can be expressed as $P_m = U_g g$ for bubble columns. Assuming that the size of the characteristic

Table 2.4: Literature Correlations for Liquid Phase Axial Dispersion Coefficient

Reference	D_{ax} (cm^2/s) (cgs units)	Range of Applicability (1 atm)
Baird and Rice (1975)	$0.35 D_c^{4/3}(U_g g)^{1/3}$	bubbly (B) and churn-turbulent (CT)
Joshi and Sharma (1979)	$0.435(g D_c(U_g - \epsilon_g u_{b\infty}))^{1/3}$ $u_{b\infty} = 23$ cm/s	B and CT
Zehner (1982)	$0.37 D_c^{4/3}(U_g g)^{1/3}$	B and CT
Ohki and Inoue (1970)	$0.3 D_c^2 U_g^{1.2}$ $14 D_c/(1-\epsilon_g)^2$	B CT
Kantak et al. (1994)	$0.2 D_c^{1.25} U_g/\epsilon_g$	B and CT
Krishna et al. (1997b)	$0.25 V_{lb} D_c$	B and CT
Deckwer et al. (1974)	$3.67 U_g^{0.32} D_c^{1.34}$	B and CT
Hikita and Kikukawa (1974)	$31.6(0.15 + 0.02 U_g^{0.77}) D_c^{1.25} \mu_l^{-0.12}$	B and CT
Towell and Ackerman (1972)	$1.22 D_c^{1.5} U_g^{0.5}$	B and CT
Berg and Schluter (1995)	$0.208 U_g^{0.4}(D_c + N_R d_R)^{1.48}$ $\phi_s^{1.8} \nu_l^{-0.12}$ (SI units) N_R: no. of tubes, d_R: o.d. of tube	B and CT internals

Table 2.5: Experimental Conditions Used for Liquid Phase Axial Dispersion Coefficient Correlations of Table 2.4

Source	D_c cm	U_g cm/s	U_l cm/s	System
Deckwer et al. (1973)	20.0	5.0 - 6.8	0.44	air-water, 1 atm
Deckwer et al. (1974)	20.0	5.0 - 12.0	0.7	"
Hikita and Kikukawa (1974)	19.0 10.0	4.0 - 34.0 4.0 - 34.0	0 0	" "
Ohki and Inoue (1970)	16.0	5.0 - 25.0	0	"
Reith et al. (1968)	14.0 29.0	7.5 - 39.0 8.0 - 45.0	1.6 "	" "
Towell and Ackerman (1972)	40.6 107.0	0.9 - 8.92	0.6 - 1.5	"
Kato and Nishiwaki (1972)	12.2	4.0 - 20.0	0.52	"
Aoyama et al. (1968)	10.0 20.0	2.0 - 7.0 0.3 - 6.5	0.18 - 0.34 0.18 - 0.62	" "
Kelkar et al. (1983)	15.4	15.0 - 25.0	0	air-water (electrolyte)

eddy is equivalent to the column diameter, D_c, Baird and Rice (1975) obtained

$$D_{ax} = K_r D_c^{\frac{4}{3}} (U_g g)^{\frac{1}{3}} \tag{2.47}$$

The constant K_r was taken to be 0.35 based on fitting of experimental data for the dispersion coefficient over a wide range of operating conditions (Table 2.5). This correlation of Baird and Rice (1975) is among the most widely used for estimating the extent of liquid backmixing in bubble columns.

There have been several approaches for evaluating the dispersion coefficient on the basis of the multiple circulation cells model (Joshi and Sharma 1979; Zehner 1982), by correlating it in terms of the mean circulation velocity. By postulating the existence of axially symmetric steady multiple circulation cells in the column and using the energy balance, Joshi and Sharma (1979) derived an expression for the average liquid circulation velocity. They correlated the liquid phase axial dispersion coefficient with the liquid recirculation velocity as

$$D_{ax} = 0.31 D_c^{1.5} u_{Lc}; \quad u_{Lc} = 1.4[D_c g(U_g - \epsilon_g u_{b\infty})]^{\frac{1}{3}} \tag{2.48}$$

indicating that the dispersion coefficient is directly proportional to the liquid recirculating velocity. The agreement of their correlation with experimental data (Table 2.5) is quite good for small diameter columns. However, the existence of such multiple cells in the time averaged sense has not been experimentally verified, which makes the physical basis questionable.

Zehner (1982) developed another multicell model as an alternative to that of Joshi and Sharma (1979), in which stationary cylindrical eddies are layered transversely above each other. For his eddy cell model Zehner showed the validity of the well known relationship (McHenry and Wilhelm 1957)

$$Pe = 2 = \frac{u_{Lc} D_c}{D_{ax}} \tag{2.49}$$

from which he arrived at an expression for the axial dispersion coefficient as

$$D_{ax} = \frac{1}{2} f^{\frac{1}{3}} D_c^{\frac{4}{3}} (U_g g)^{\frac{1}{3}} \tag{2.50}$$

Using experimental data for D_{ax} from the literature, the friction factor f was fitted to a value of 0.398. The final expression for the axial dispersion coefficient is similar to that of Baird and Rice (1975) (Table 2.4).

Recently, Millies and Mewes (1995) showed that liquid recirculation in bubble columns is a flow instability caused by a disturbance, or non-uniformity, of gas distribution, and thereby calculated the flow field as consisting of several steady circulation cells, similar to the postulate of Joshi and Sharma (1979). In the presence of such cells, they emphasize the importance of the region between cells where the resistance to the transport of tracer is the greatest. Assuming that within a cell or vortex the tracer is well mixed, a simplified diffusion type of equation is obtained for the concentration variation between different cells, from the original transport equation for the tracer, which corresponds to the one dimensional dispersion model equation. The dispersion coefficient calculated on this basis was shown to compare well with the dispersion coefficient of Zehner (1982). They further proceed to develop a structured model using the recirculating cell model, based on which they show that the axial dispersion coefficient is directly proportional to the liquid recirculating velocity, as argued by Zehner (1982) and Joshi (1980). No correlation was developed.

The basic framework of the analyses of Joshi and Sharma (1979), Zehner (1982) and Millies and Mewes (1995) is the same, with regard to the existence of multiple circulation cells. If one assumes the existence of such stationary cells, the analysis presented for each case is acceptable. However, experimental information on the time averaged flow patterns in bubble columns (Devanathan 1991; Franz et al. 1984) clearly indicates that the presence of these cells is questionable. The instantaneous flow pattern does exhibit the presence of eddies and vortical structures (Chen et al. 1994). These structures are highly transient and get averaged out, resulting in global liquid recirculation in the time averaged sense, which does not exhibit multiple cells.

Groen et al. (1996) attempted to develop a physical basis for the axial dispersion coefficient using the concept of the 'swarm velocity'. They utilized a glass fiber (optical) probe to measure the local gas holdup in the column. In addition, by simultaneously using probes positioned at two axial positions, they applied cross-correlation techniques to study the dynamics of the flow. At low gas flow rates they estimated the life time of an eddy to be about 0.5 sec and the length scale in the axial

direction to be the size of the column diameter. They showed that at low gas velocities the flow can be characterized by a single dominant swarm velocity. It appears that, based on the radial position of measurement, the probes were capturing the maximum upward and down velocities. In this view the axial dispersion coefficient was modeled as:

$$D_{ax} = K_g u D_c \tag{2.51}$$

where u is the swarm velocity, which for low superficial gas velocities is claimed to be a constant. The constant K_g was assumed to be unity. The results of the above model were shown to compare well with experimental data for D_{ax}, at low superficial gas velocities in the homogeneous bubbly flow regime. At higher gas flow rates in the churn-turbulent flow regime it is expected that several scales and frequencies will be dominant, so that the above approach is questionable.

Krishna et al. (1997b) considered the axial dispersion coefficient to be proportional to the product of the centerline liquid velocity and a length scale which is equal to the column diameter. In the churn-turbulent flow regime, they concluded that the liquid recirculation velocity is directly proportional to the rise velocity of the large bubbles, and arrived at the following expression for the axial dispersion coefficient:

$$D_{ax} = 0.25 V_{lb} D_c \tag{2.52}$$

where V_{lb} is the rise velocity of large bubbles (Table 2.2). The constant in the above equation is estimated by fitting experimental data. It seems, however, that the above expression over-predicts the experimental axial dispersion coefficient (Krishna et al. 1997b).

In contrast to the above theories, which relate the axial dispersion coefficient to an effective liquid velocity, Riquarts (1981) attributes the axial dispersion coefficient to arise only from stochastic mixing caused by the motion of the rising bubbles, and not from circulation. In his analysis, he uses a mass balance during a steady state experiment, by considering liquid upflow in the core and downflow in the annular

portion of the bubble column. He assumes that the tracer concentrations in the core region and annular regions are identical and neglects radial diffusion, leading to an oversimplification of the model equations. As a result, he shows that the axial dispersion coefficient appearing in the one dimensional axial dispersion model has contributions only from stochastic mixing (or the axial eddy diffusion). This is physically counter-intuitive, since it is well established that the large degrees of liquid backmixing in bubble columns are a result of liquid recirculation. The final expression for the axial dispersion coefficient obtained is given by:

$$\mathrm{Bo} = 14.7(\frac{\mathrm{Fr}^3}{\mathrm{Re}})^{0.125} \tag{2.53}$$

where $\mathrm{Bo} = U_g D_c/D_{ax}$, $\mathrm{Fr} = U_g^2/(D_c g)$ and $\mathrm{Re} = U_g D_c/\nu_l$.

Wilkinson et al. (1993) formulated a mechanistic model to account for liquid mixing in bubble columns caused by convection along with axial dispersion and radial turbulent exchange. The objective was to study the effect of pressure on liquid backmixing. By making several simplifying assumptions in their model, they arrived at an expression for the dispersion coefficient in terms of the convective liquid velocity, axial turbulent dispersion and radial exchange term. However, due to the unknown values of the turbulent dispersion coefficient and exchange factor K (which is a function of operating conditions) quantitative estimates of the dispersion coefficient using this expression could not be made. They experimentally measured the liquid phase dispersion coefficient in air-water systems at high pressure, and showed that there is an increase in D_{ax} with pressure. The existing literature correlations were shown to under-predict the axial dispersion coefficient under high pressure conditions. Additional details regarding experimental results of Wilkinson et al. (1993) are discussed in Chapter 6.3 along with the present analysis for estimating the contributions of various factors to overall liquid backmixing in bubble columns.

Kantak et al. (1994) recently tried to improve on the existing correlations for estimating the axial dispersion coefficients for a wide range of systems. Adopting the analogy of dispersivity in porous media, they define the dispersivity for the liquid

phase in bubble columns as the ratio of the dispersion coefficient to the phase velocity. For the case of bubble column flows the intrinsic gas velocity, $\frac{U_g}{\epsilon_g}$, was used as the phase velocity, since it is the controlling velocity. Using experimental data over a wide range of conditions (Table 2.5 and others), they arrived at the following correlation for the liquid axial dispersion coefficient:

$$\frac{D_{ax}}{(U_g/\epsilon_g)} = 0.2D_c^{1.25} \tag{2.54}$$

The database considered by Kantak et al. (1994) in arriving at their correlation, is a very broad database (liquids of different properties including the presence of solids). Having taken into consideration various conditions, they claim that their correlation provides the best fit on the basis of the overall standard error. However, when used for predicting the dispersion coefficient in a laboratory scale unit with air and water, it appears that their correlation considerably over-predicts the axial dispersion coefficient. It seems that their correlation cannot capture the variation in the fluid dynamics that occurs due to the influence of physical properties and its effect on liquid mixing. In addition, their correlation is unsuitable for high pressure systems, since it predicts the opposite trends for the axial dispersion coefficient, when compared with experimental data of Wilkinson et al. (1993). An increase in pressure results in an increase in the gas holdup and an increase in the axial dispersion coefficient. In Equation 2.54 the gas holdup is inversely proportional to the dispersion coefficient, and therefore, shows a decrease in the axial dispersion coefficient with increase in pressure (and gas holdup).

In order capture the effect of system properties and operating conditions such as pressure and temperature on liquid mixing, it is necessary to first study these effects on the fluid dynamics and thereafter the effects of fluid dynamics on liquid backmixing in bubble columns. Such an analysis has been performed as part of this work and is described in Chapter 5 and Chapter 6.3.

Most of the existing correlations for the axial dispersion coefficient are developed for air-water systems at atmospheric conditions. As a result, these correlations

severely under-predict the axial dispersion coefficient in industrial bubble column reactors that operate under high pressure conditions (discussed in Chapter 6.3), and can not be applied to such conditions. In addition, a majority of industrial systems have internal heat exchanger tubes, which have also been shown to increase the axial dispersion coefficient (Berg et al. 1995). To account for the effects of the heat exchanger tubes Berg et al. (1995) propose a correlation, shown in Table 2.4. This correlation has been tested against experimental tracer data considered in this investigation, in an industrial slurry bubble column reactor, and is discussed in greater detail in Chapter 6.3.

Several attempts have been made in performing a Taylor type analysis to arrive at an expression for the axial dispersion coefficient. Mashelkar and Ramachandran (1975) derived an expression by assuming negligible axial turbulent diffusivity, for viscous chain bubbling. The flow regime for applicability of their expression is not of interest in the present investigation. Ohki and Inoue (1970) developed a dispersion model in the bubbly flow regime, by essentially modifying the Taylor-Aris approach. Assuming a uniform turbulent diffusivity in the column, they arrived at an expression for the dispersion coefficient in the bubbly flow regime (Table 2.4). In the churn-turbulent flow regime the model parameters could not be directly evaluated from first principles.

Miyauchi et al. (1981) considered the effects of the radial profile of the recirculating velocity (Ueyama and Miyauchi 1979), along with radial and axial turbulent diffusion, in estimating the axial dispersion coefficient. The drawback of their analysis was that a constant gas holdup was assumed throughout the cross-section of the column. This was shown, by Myers (1986), to lead to inconsistencies in the flow equations. Anderson (1989) in a similar type of analysis assumed an average gas holdup instead of a profile, and in addition neglected the axial eddy diffusivity. It is apparent from the present analysis and experimental results reported in Chapter 6.3, that the axial eddy diffusivity has a considerable contribution to the liquid axial dispersion coefficient.

Despite the various attempts at using a theoretical or semi-theoretical approach in obtaining an expression for the axial dispersion coefficient, there still exists no relationship that allows the quantification of the contributions of the different mechanisms to overall backmixing. In the present work such a quantification has been made, by adopting a Taylor type analysis and using experimental data from CARPT measurements for the various fluid dynamic quantities. A detailed analysis along with results is presented in Chapter 6.3. This quantification of the contributions of various fluid dynamic parameters to the axial dispersion coefficient is applied, along with the scale-up methodology proposed in Chapter 5, to study the effects of pressure, presence of internals, etc., on the overall liquid backmixing in bubble columns.

2.4.2 Alternate Mixing Models

In order to improve upon the axial dispersion model and obtain a better description of liquid mixing in bubble columns, several phenomenological models have been developed in the past. Some of these models have already been described in the previous section while presenting the different approaches attempted in the literature to evaluate the axial dispersion coefficient.

Myers et al. (1986) proposed a slug and cell model for the churn-turbulent regime in bubble columns. The model considers the system to be divided into gas rich regions called slugs and gas lean regions called cells. The slugs move upwards along the center of the column, entrain and transport liquid to various points within the system. The cells are stationary and vigorously agitated by the passage of the slugs. The model originally has six parameters, but using simplifying assumptions can be transformed to a single parameter model. Model predictions were shown to compare well with experimental tracer response data for small columns (19 cm diameter). The basis of the model, which assumes a series of slugs passing through a single row of stationary cells, may not hold for larger diameter columns.

Deckwer and Schumpe (1987) presented a zone model for the liquid. This model assumes plug flow of the liquid in the central region of the column, where the

liquid is entrained in the large bubbles rising straight up the column. The upflowing liquid then descends at the walls. This is represented by a series of cells with back-flow between the cells. There is also radial exchange between upflow and downflow. Due to a lack of a method for estimating the exchange and back-flow coefficients, the zone model has not been successfully applied to bubble columns. The recycle and cross-flow model of Hochman and McCord (1970), which was originally developed for tubular reactors with large length to diameter ratios, is another similar type of model which is suitable for modeling liquid mixing in bubble columns. An extended version of this model is discussed in Chapter 6.2. The classical mixing cells model with backflow was used by Turner and Mills (1990) for modeling slurry bubble columns, and it was shown that the results were similar to that of the ADM.

Rustemeyer et al. (1989) developed a mixing model based on the convective recirculating velocity profile with superimposed turbulent diffusion. The random fluctuations generated by the motion of the vortical structures in the column were accounted for by passage of the liquid velocity profile through stationary stirred tanks which are ideally mixed. This approach is similar to that of Myers et al. (1986). The solution of the model equation, requires fitting of two parameters, the turbulent diffusion coefficient and the number of perfectly mixed cells in the column.

In the present work, a fundamental description of liquid mixing is derived by considering the basic two-fluid model equations for tracer species balance, in a two dimensional axisymmetric domain. This essentially results in a convective-diffusion equation. Using the fluid dynamic information measured as part of this work, the model is solved to predict tracer distribution in the column. Unlike other models discussed so far, no fitting parameters are required for the proposed model since all the input parameters can be obtained using experimental measurements from CARPT and CT. Scale-up methodologies are suggested to scale the model parameters in order to use the model for an industrial slurry bubble column reactor (Chapter 5). The original two dimensional model is then simplified to arrive at a one dimensional

phenomenological description for liquid mixing, where it is shown that the model parameters can be directly obtained from experiment.